JPE 4-4-2

A Self-Excited Induction Generator with Simple Voltage Regulation Suitable for Wind Energy

Tarek Ahmed†, Katsumi Nishida* and Mutsuo Nakaoka*

The Graduate School of Science and Engineering, Yamaguchi University, Yamaguchi, Japan

ABSTRACT

In this paper, a three-phase induction machine-based wind power generation scheme is proposed. This scheme uses a low-cost diode bridge rectifier circuit connected to an induction machine via an ac load voltage regulator (AC-LVR) to regulate dc power transfer. The AC-LVR is used to regulate the DC load voltage of the diode bridge rectifier circuit which is connected to the three-phase self-excited induction generator (SEIG). The excitation of the three-phase SEIG is supplied by the static VAR compensator (SVC). This simple method for obtaining a full variable-speed wind turbine system by applying a back-to-back power converter to a wound rotor induction generator is useful for wind power generation at widely varying speeds. The dynamic performance responses and the experimental results of connecting a 5kW 220V three-phase SEIG directly to a diode bridge rectifier are presented for various loads. Moreover, the steady-state simulated and experimental results of the PI closed-loop feedback voltage regulation scheme prove the practical effectiveness of these simple methods for use with a wind turbine system.

Keywords: Self-excited induction generator, Static VAR compensator, AC load voltage regulator

1. Introduction

By adjusting the value of the excitation capacitance or the prime mover speed, one can maintain a constant output voltage for a three-phase self-excited induction generator (SEIG) with variable loads. However, adjusting the prime mover speed is not always possible. So, the appropriate method is to continuosly adjust the capacitor value[1]-[2]. Adjusting the excitation capacitor value can be achieved by many control strategies using power electronic technology[3-9].

Manuscript received May 26, 2004; revised July 14, 2004.

†Corresponding Author: tarek@pe-news1.eee.yamaguchi-u.ac.jp
Tel: +81-836-85-9472, Fax: +81-836-85-9401, Yamaguchi Univ.
*Division of Electrical and Electronics Eng, Yamaguchi Univ.

Some of these proposals use inverters and field-orientation algorithms to excite and control the induction generator. These proposals enable strict voltage regulation and high efficiency. However, field orientation requires costly and unreliable mechanical position sensing systems of encoders or resolvers. There are other proposals that do not require position-sensing systems. Some of them are based on a shunt-connected PWM voltage source inverter which supplies constant frequency voltage. Others supply reactive current to the induction generator by using a capacitor bank and an inverter simultaneously. These are based on the instantaneous reactive power theory[8]-[9].

Based on no-load and full-load conditions, the *d–q* model is used to provide the complete solution and transient and steady-state analyses of the three-phase

SEIG with a diode bridge rectifier circuit. Moreover, a simple stand-alone dc power supply for use in rural districts is presented. This promising supply is composed of the three-phase SEIG driven by a variable-speed prime mover (VSPM) with an ac load voltage regulator (AC-LVR) and a low-cost diode bridge rectifier circuit. The steady-state simulated and experimental results of the closed-loop feedback system with a PI controller, using an AC-LVR, are calculated and discussed for the stand-alone dc utilizations.

2. System configuration

Figure 1 illustrates a wind power generation DC supply based on a simple method for obtaining a full variable-speed wind turbine system. It uses a bi-directional power converter connected to a conventional wound rotor induction generator. The schematic system configuration of the VSPM coupled three-phase SEIG with AC-LVR and PI controller voltage regulation scheme in the feedback control loop is shown in Fig.1. The PI controller circuit and the thyristors phase angle control circuit are designed for this scheme. Table I indicates the design specifications and the induction machine parameters of the three-phase SEIG and the constant circuit parameters of the voltage regulation system.

The circuit in Fig.1 represents an application of the ac voltage controller to regulate a dc load voltage using a low-cost diode bridge rectifier directly connected to the three-phase SEIG via the AC-LVR. This scheme regulates the voltage for a prime mover such as a wind turbine which operates at a wide range of speeds. The reactive power, generally required for generating the rated voltage at the rated speed is provided by using a static VAR compensator composed of a fixed excitation capacitor (FC) and a thyristor controlled capacitor (TSC). At low speed, additional reactive power is required from the TSC. However, an AC-LVR is required to regulate the load voltage.

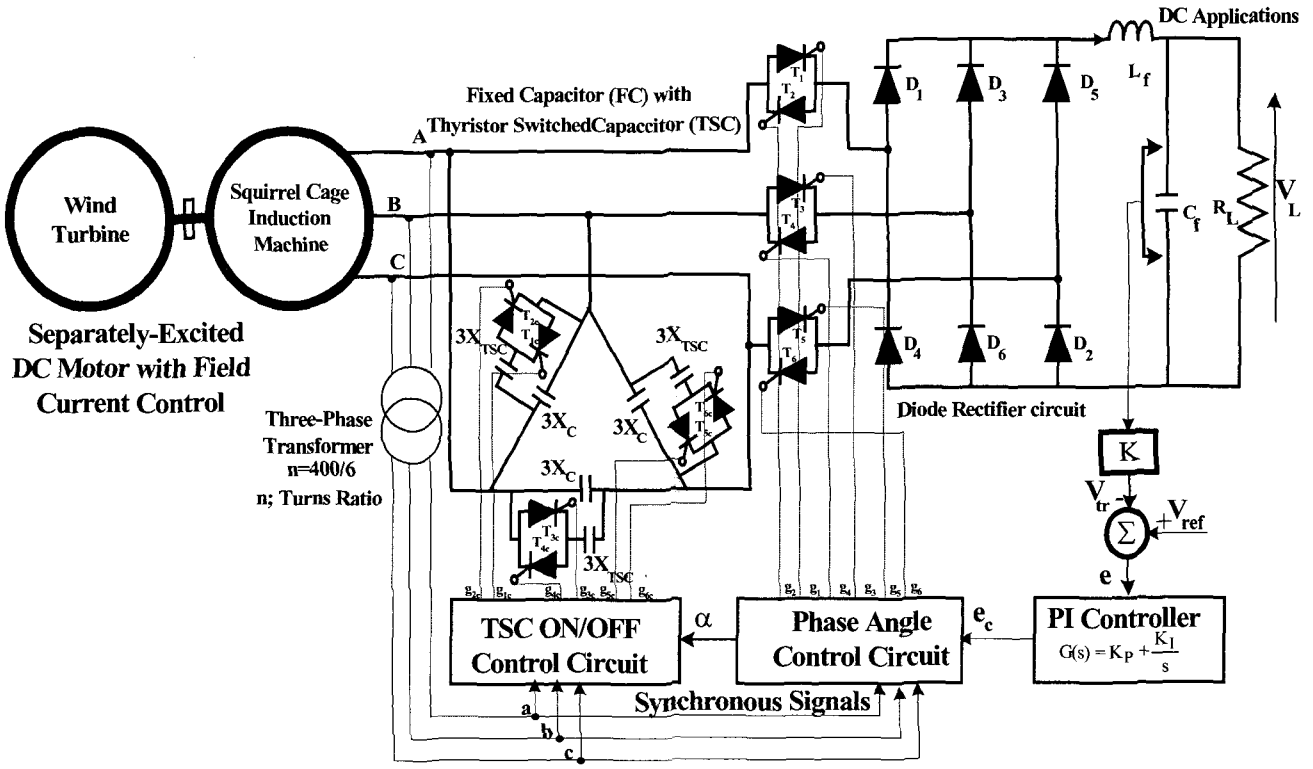

Fig.1 System configuration of a three-phase SEIG driven by a VSPM with an AC-LVR and a PI controller

Table 1 Design Specifications and Circuit Parameters

Items	Machine Rating and Machine Parameters	
Three-Phase Star Connected Induction Machine	Rated Voltage	220 V
	Rated Power	5 kW
	Number of Poles	4
	Rated Frequency	60 Hz
	Rotor Type	Wound Rotor
	Induction Machine Parameters at 60 Hz	
	R_s=0.6 Ohm	X_{ls}=1.375 Ohm
	R_r=0.6 Ohm	X_{lr}=1.375 Ohm
SVC (FC & TSC)	X_C; C	200 μF
	X_{TSC}; C_{TSC}	50 μF
PI Controller	K_P	0.38
	K_I	12.5
Low Pass Filter	C_F	3300 μF
	L_F	100 mH

3. SEIG with Diode Bridge Rectifier Circuit

A three-phase SEIG model is helpful for analyzing the generator's characteristics. First, the parameters of the three-phase SEIG need to be calculated for the model. The traditional tests used to get the parameters for a three-phase SEIG equivalent circuit model are the open-circuit (no load) test and the short-circuit (locked rotor) test [1-3]. For induction machines used in motorized applications, it is important to determine the magnetizing reactance at its rated voltage. Variation of the magnetizing reactance is the main parameter affecting the dynamics of voltage buildup and stabilization for a three-phase SEIG. To determine the magnetization curve of the three-phase induction machine, it is driven at the synchronous speed of N_S=1800 r/min and a variable ac supply voltage is applied to the stator winding at the rated frequency of 60Hz. The relation between the magnetizing reactance X_m and the magnetizing current I_m is obtained experimentally. It is depicted in Fig.2. The magnetization curve obtained experimentally is represented by the fourth order curve fit as follows,

$$X_m = -11 \times 10^{-2} I_m^4 + 2.4 I_m^3 - 18.58 I_m^2 + 57.05 I_m - 3 \quad (1)$$

The d–q model of the three-phase SEIG with a diode bridge rectifier circuit, shown in Fig. 3, is used because it provides the complete solution, both transient and steady state, of the self-excitation process. The parameters obtained from the tests at rated values of voltage and frequency are L_{ls}=L_{lr}=3.7 mH, R_s=0.6 , and R_r=0.6 . The d–q-axes equivalent circuits of an induction machine with a diode bridge rectifier circuit in a stationary reference frame are given in Fig. 3. The dynamic model of the induction machine in the stationary reference frame is described by the following equations[9]. The simulation was carried out by solving the first-order differential equation, derived on the basis of the no-load condition from Fig. 3, for the three-phase SEIG given by,

$$pI = AI + B \quad (2)$$

where $I = \begin{bmatrix} i_{qs} \\ i_{ds} \\ i_{qr} \\ i_{dr} \end{bmatrix}$,

$$A = \frac{1}{\delta} \begin{bmatrix} -L_r R_s & -\omega_r L_m^2 & L_m R_r & -L_m \omega_r L_r \\ \omega_r L_m^2 & -L_r R_s & L_m \omega_r L_r & L_m R_r \\ L_m R_s & L_m \omega_r L_s & -L_s R_r & L_s \omega_r L_r \\ -L_m \omega_r L_s & L_m R_s & -L_s \omega_r L_r & -L_s R_r \end{bmatrix}$$

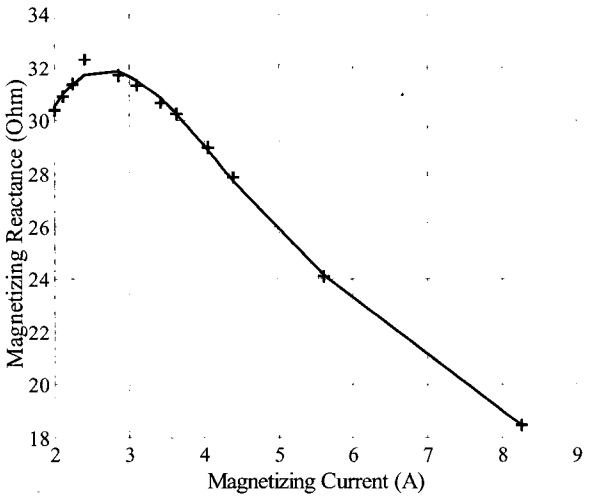

Fig. 2 Magnetizing reactance versus magnetizing current of three-phase induction machine

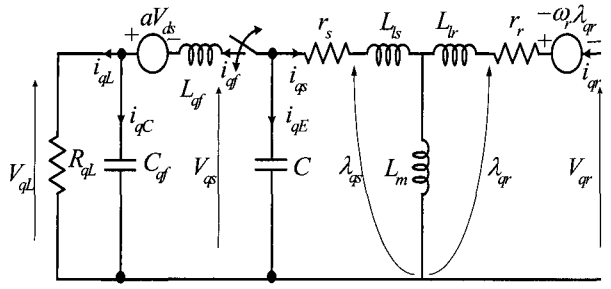

(a) q-axis

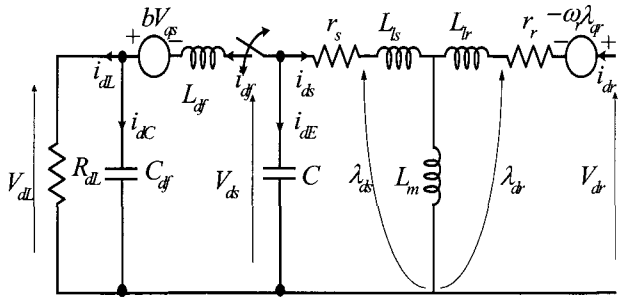

(b) d-axis

Fig. 3 d–q model of a SEIG with a diode bridge rectifier circuit, a low pass filter, a DC load and a fixed excitation capacitor in a stationary reference frame

$$B=\frac{1}{\delta}\begin{bmatrix} L_r & 0 & -L_m & 0 \\ 0 & L_r & 0 & -L_m \\ -L_m & 0 & L_s & 0 \\ 0 & -L_m & 0 & L_s \end{bmatrix}\begin{bmatrix} V_{qs} \\ V_{ds} \\ V_{qr} \\ V_{dr} \end{bmatrix}$$

$$\delta=(L_sL_r-L_m^2),$$

$$L_m=\frac{X_m}{120\pi}$$

and $p=\dfrac{d}{dt}$

The d–q-axes equivalent circuit models of a diode bridge rectifier circuit, a low pass filter, a DC load and a fixed excitation capacitor in a stationary reference frame are defined by,

$$p\begin{bmatrix} v_{qs} \\ v_{ds} \\ v_{qL} \\ v_{dL} \end{bmatrix}=\frac{1}{C}\begin{bmatrix} -1 & 0 & -1 & 0 \\ 0 & -1 & 0 & -1 \\ 0 & 0 & \dfrac{C}{C_{qf}} & 0 \\ 0 & 0 & 0 & \dfrac{C}{C_{df}} \end{bmatrix}\begin{bmatrix} i_{qs} \\ i_{ds} \\ i_{qf} \\ i_{df} \end{bmatrix}-\begin{bmatrix} 0 \\ 0 \\ \dfrac{v_{qL}}{C_{qf}R_{qL}} \\ \dfrac{v_{dL}}{C_{df}R_{dL}} \end{bmatrix} \quad (3)$$

$$p\begin{bmatrix} i_{qf} \\ i_{df} \end{bmatrix}=\frac{1}{L_{qf}L_{df}}\left\{\begin{bmatrix} L_{df} & aL_{df} \\ bL_{qf} & L_{qf} \end{bmatrix}\begin{bmatrix} v_{qs} \\ v_{ds} \end{bmatrix}-\begin{bmatrix} L_{df}v_{qL} \\ L_{qf}v_{dL} \end{bmatrix}\right\} \quad (4)$$

The pair of diodes, which are connected between that pair of three-phase SEIG lines having the highest amount of instantaneous line-to-line voltage, will conduct. The operation modes will indicate in the following tables. Table I indicates the q-d axes parameters of the diode rectifier circuit, the low pass filter and the DC load in stationary reference frame as shown in Fig.3 when the highest value of the instantaneous line-to-line voltage of the three-phase SEIG is V_{ab} or the absolute value $|V_{ab}|$.

Table 2 Highest Instantaneous Line Voltage (V_{ab} AND $|V_{ab}|$)

***q*-axis**	***d*-axis**
$a=\dfrac{1}{\sqrt{3}}$	$b=\sqrt{3}$
$L_{qf}=\dfrac{2}{3}L_f$	$L_{df}=2L_f$
$C_{qf}=\dfrac{3}{2}C_f$	$C_{df}=\dfrac{\sqrt{3}}{2}C_f$
$R_{qL}=\dfrac{2}{3}R_L$	$R_{dL}=\dfrac{2}{\sqrt{3}}R_L$
If V_{ca} < V_{ab} > V_{bc} ; $V_L=\dfrac{3}{2}V_{qL}$ If $\lvert V_{ca}\rvert$ < $\lvert V_{ab}\rvert$ > $\lvert V_{bc}\rvert$; $V_L=-\dfrac{3}{2}V_{qL}$	If V_{ca} <V_{ab} > V_{bc} ; $V_L=\dfrac{\sqrt{3}}{2}V_{dL}$ If $\lvert V_{ca}\rvert$ < $\lvert V_{ab}\rvert$ > $\lvert V_{bc}\rvert$; $V_L=-\dfrac{\sqrt{3}}{2}V_{dL}$

When the highest value of the instantaneous line-to-line voltage of the three-phase SEIG is V_{ca} or the absolute value $|V_{ca}|$, the q-d axes equivalent circuit parameters are

the same as indicted in Table I, except for the following parameters listed in Table III,

Table 3 Highest Instantaneous Line Voltage (V_{ca} AND $|V_{ca}|$)

q-axis	*d*-axis
$a=-\frac{1}{\sqrt{3}}$	$b=-\sqrt{3}$
If $V_{ab} < V_{ca} > V_{bc}$; $V_L=-\frac{3}{2}V_{qL}$ If $\|V_{ab}\| < \|V_{ca}\| > \|V_{bc}\|$; $V_L=\frac{3}{2}V_{qL}$	If $V_{ab} < V_{ca} > V_{bc}$; $V_L=\frac{\sqrt{3}}{2}V_{dL}$ If $\|V_{ab}\| < \|V_{ca}\| > \|V_{bc}\|$; $V_L=-\frac{\sqrt{3}}{2}V_{dL}$

If the highest value of the instantaneous line-to-line voltage of the three-phase SEIG is V_{bc} or the absolute value $|V_{bc}|$, the q-axis current i_{qf} equals zero, which means that the q-axis equivalent circuit model of the diode rectifier circuit, the filter and the DC load are disconnected. The d-axis equivalent circuit parameters are indicted in Table IV.

Table 2 Highest Instantaneous Line Voltage (Vbc AND |Vbc|)

d-axis			
$b=0$	$L_{df}=\frac{1}{2}L_f$	$C_{df}=2C_f$	$R_{dL}=\frac{2}{\sqrt{3}}R_L$
$V_L=-\sqrt{3}V_{dL}$, when $V_{ab} < V_{bc} > V_{ca}$			
$V_L=\sqrt{3}V_{dL}$, when $\|V_{ab}\| < \|V_{bc}\| > \|V_{ca}\|$			

4. Simulation and Experimental Results for a SEIG with Diode Bridge Rectifier Circuit

To study the induction generator, directly connected to the full-bridge diode rectifier circuit for a dc application, the d-q model is derived as explained in the previous section. The dc load is connected to the machine terminals via a filter inductor L_f, and a capacitor C_f to reduce the harmonics injected into the machine, thereby reducing the output voltage harmonics of the machine. The excitation to the machine is supplied by means of a fixed excitation capacitor (C =200 μ F).

4.1. No-Load Operation

To investigate the characteristics of the dynamic stator current and the generated voltage of the three-phase SEIG, the input diode rectifier current(which equals zero) and the output diode rectifier voltage are simulated. The current and voltage are measured while the speed is kept at a constant value(N=1530 r/min) by a controllable separately excited dc motor, which is used as a prime mover for the three-phase SEIG. The simulated results of the dynamic stator current, the voltage of the three-phase SEIG and the output voltage of the rectifier circuit are given in Fig. 4. The experimental results are given in Fig. 5.

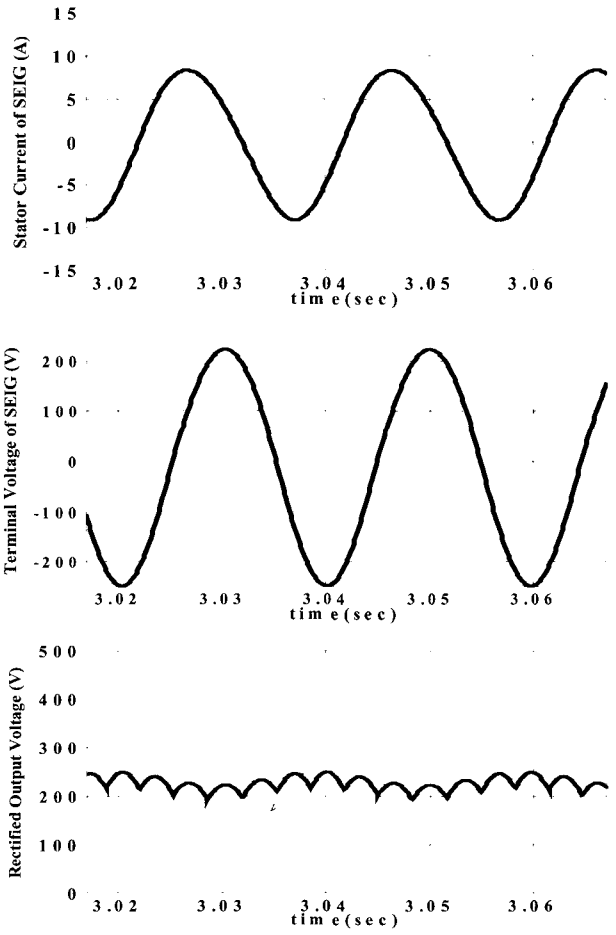

Fig. 4 Simulation results of the stator current of the SEIG, generated voltage of the SEIG, and the rectified output voltage

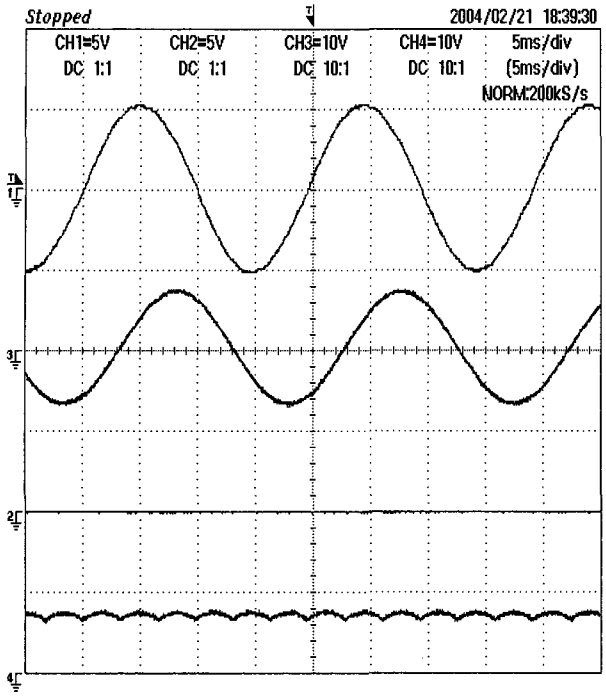

Fig. 5 Experimental results of the stator current of the SEIG, generated voltage of the SEIG and the rectified output voltage

4.2 Full-Load Operation

Fig. 6 indicates the simulation results of the dynamic stator current of the three-phase SEIG, the generated voltage of the three-phase SEIG, the input diode rectifier current and the output diode rectifier voltage, all of which vary according to the load applied. The generated frequency and the dc load voltage are dependent upon the input current of the diode rectifier circuit variations. Fig. 7 indicates the corresponding experimental results for the circuit. An increase in the load current will decrease the generated voltage and its frequency. The simulation results are given in Fig. 8. The THD of the three-phase SEIG stator current is exaggerated due to a change in the dc load where it is measured to 7% with the full load. Increasing the capacitance can compensate for the generated voltage, but this increases the stator current. Hence, care should be taken not to exceed the stator rated current.

To develop an electronic power control system which will regulate the generated voltage for a dc load over a wide range of speeds one must meet all of the above conditions.

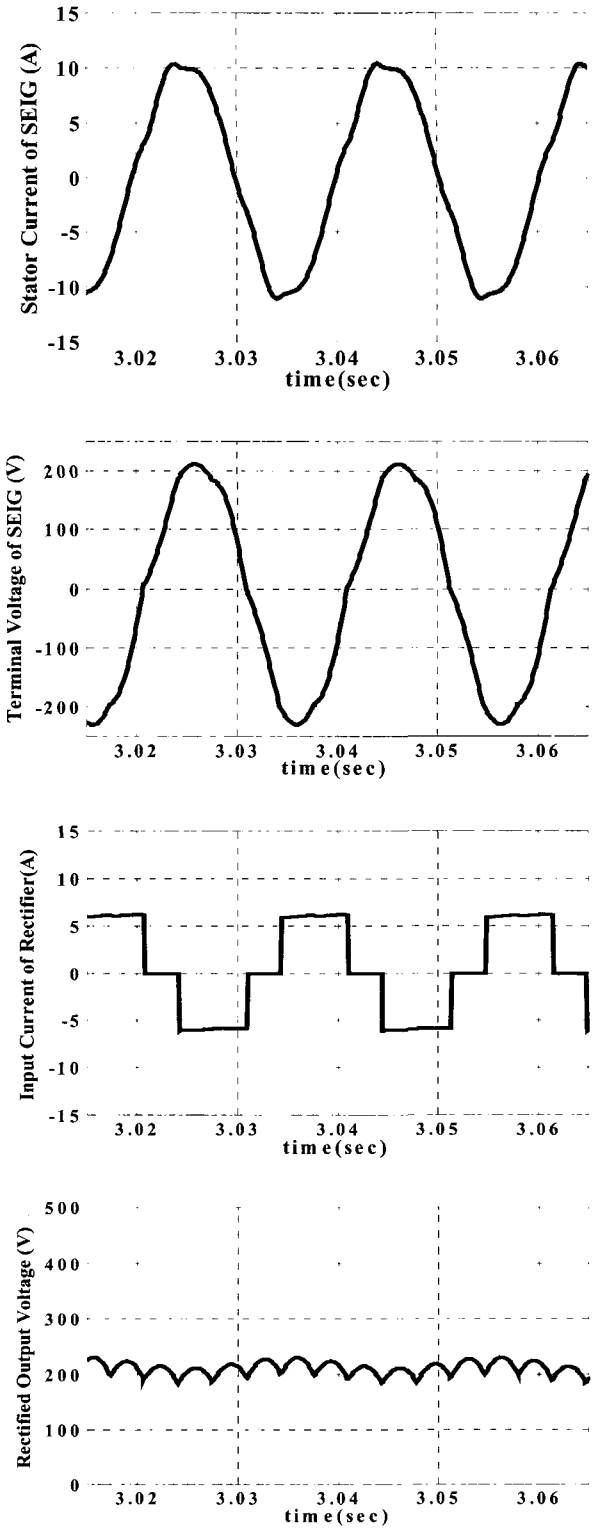

Fig. 6 Simulation results of the stator current of the SEIG, generated voltage of the SEIG, input current of the diode rectifier and rectified output voltage

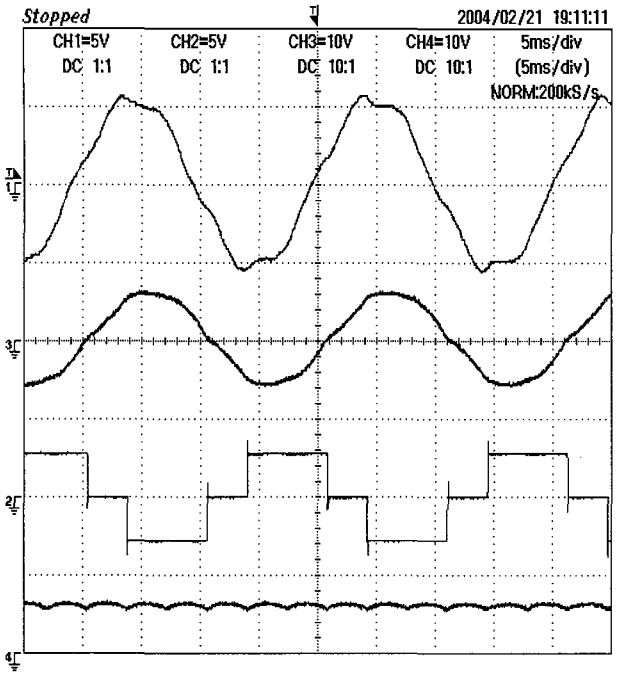

Fig. 7 Experimental results of the stator current of the SEIG, generated voltage of the SEIG, input current of the diode rectifier and rectified output voltage

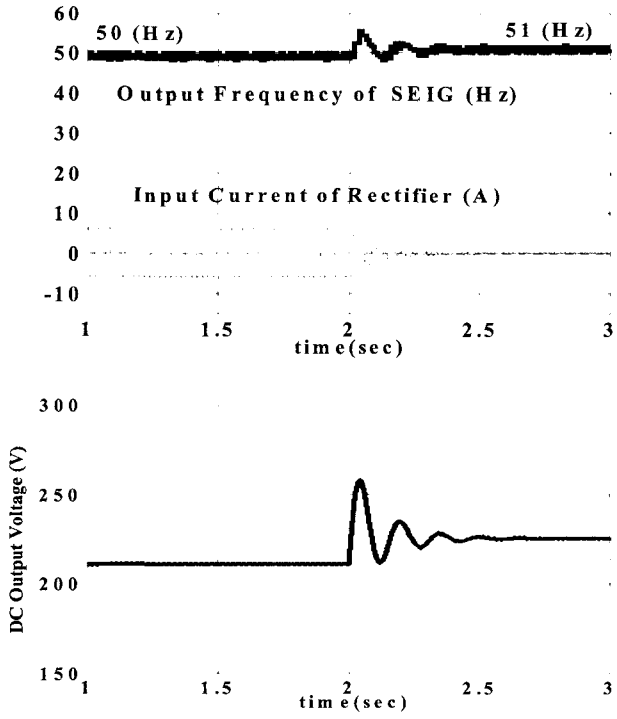

Fig. 8 Simulation results of the generated frequency and dc load voltage with the input current variations of the diode rectifier circuit

5. Per-Unit Frequency and Per-unit Speed of SEIG Driven by VSPM

The per-phase approximate equivalent circuit of the three-phase SEIG, excited by the SVC and AC-LVR, is depicted in Fig.9[1-7]. The equivalent DC load representing the three-phase SEIG terminal ports and the capacitive reactance X_{TSC} of the TSC is connected in parallel with the fixed excitation reactance X_C[2]-[10].

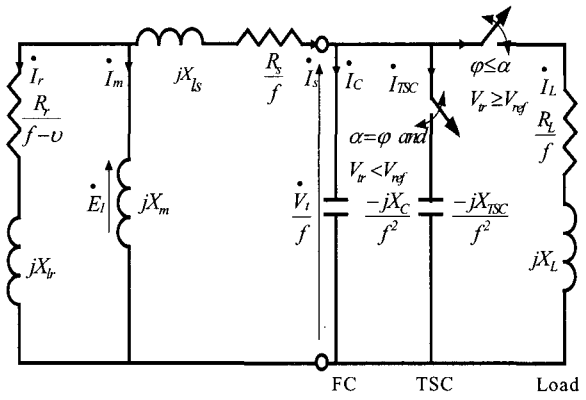

Fig.9 Per-phase equivalent circuit of the SEIG with SVC and AC-LVR in steady-state

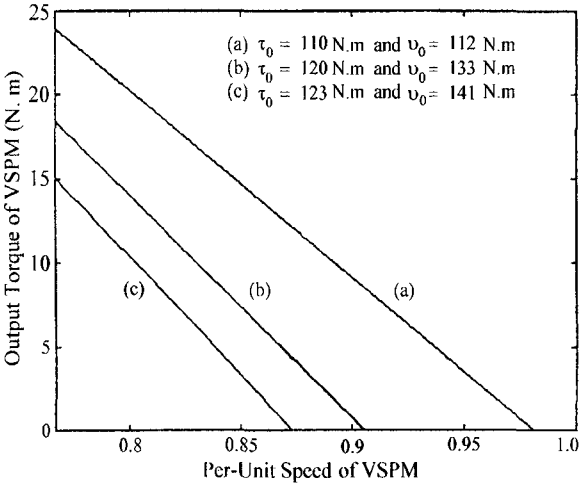

Fig.10 Mechanical output torque-speed characteristics of the VSPM

The term $(f\text{-}\upsilon)$ is extremely small. As a result, the term (X_{lr}^2) can be ignored with respect to $[R_r^2/(f\text{-}\upsilon)^2]$. The mechanical input power, P_i of the three-phase SEIG can be written as [2],

$$P_i = -3\frac{E_1^2}{R_r}\left(\frac{f-\upsilon}{f}\upsilon\right) \quad (5)$$

where E_1 is the air gap voltage per phase and f is the per unit frequency(f=F/60.0, F is the output frequency of the SEIG).

The mechanical output power, P_m of the VSPM is defined as [6]-[7],

$$P_m = (\tau_o - \upsilon_o\upsilon)\omega_s\upsilon \quad (6)$$

where υ(υ=N/N_s) is the per unit speed of the VSPM, N is the rotor speed, N_s is the three-phase SEIG rated synchronous speed in r/min, ω_s is the rated synchronous angular speed, τ_o is the torque coefficient, and υ_o is the speed coefficient. In the experiment, a controllable dc motor is used with a constant armature voltage and a field current control. Fig.10 illustrates the effect of the field current control on the torque-speed characteristics and the corresponding torque-speed coefficients of the VSPM.

By equating (5) to (6) to create a mechanical power balance, the per unit speed υ can be obtained as follows:

$$\upsilon = \frac{R_2\omega_s\tau_0 + 3E_1^2}{R_2\omega_s\upsilon_0 f + 3E_1^2} f \quad (7)$$

6. Steady State Analysis of SEIG with SVC and AC-LVR

By applying the impedance approach to the three-phase SEIG terminal ports, where the SEIG circuit has been replaced by its approximate circuit and DC load equivalent, as shown in Fig.9, the following equation can be defined as,

$$\dot{Z}_{rm} + \dot{Z}_{mq} + \dot{Z}_{qr} = 0 \quad (8)$$

where $\dot{Z}_{rm}$, $\dot{Z}_{mq}$ and $\dot{Z}_{qr}$ are described by considering the equivalent circuit shown in Fig. 9 and defined as (A1), (A2) and (A3), respectively, in the Appendix.

The two non-linear simultaneous equations of the magnetizing reactance X_m are obtained by equating the imaginary and real parts of (8) to zero and arranging as follows,

$$X_m = -\frac{C_0 + C_1 f + C_2 f^2 + C_3 f^3 + C_4 f^4 + C_5 f^5}{(A_0 + A_1 f + A_2 f^2 + A_3 f^3 + A_4 f^4)f} \quad (9)$$

$$X_m = \frac{D_0 + D_1 f + D_2 f^2 + D_3 f^3 + D_4 f^4 + D_5 f^5}{(B_0 + B_1 f + B_2 f^2 + B_3 f^3 + B_4 f^4)f} \quad (10)$$

Through equating (9) and (10), the ninth degree polynomial equation is derived by,

$$Y_9 f^9 + Y_8 f^8 + Y_7 f^7 + Y_6 f^6 + Y_5 f^5 + Y_4 f^4 + Y_3 f^3 + Y_2 f^2 + Y_1 f + Y_0 = 0 \quad (11)$$

where the real coefficients from Y_0 to Y_9 expressed in terms of constants A_i (i=0~4), B_j (j=0~4), C_k (k=0~5) and D_l (l=0~5) are indicated in the Appendix.

By using the Newton Raphson method with the initial value of the per-unit frequency f=τ_0/υ_0, the per-unit frequency f can be determined from (11). The magnetizing reactance X_m is calculated by substituting the per-unit frequency f into (9) or (10). The air gap voltage E_1 is evaluated from (1).

By neglecting the harmonics, the three-phase SEIG results calculated by using the equivalent circuit for each phase shown in Fig. 9, are given as follows,

The per-phase output voltage of the three-phase SEIG is defined as,

$$V_t = fE_1\frac{\left|\dot{Z}_{qr}\right|}{\left|\dot{Z}_{qr} + \dot{Z}_{mq}\right|} \quad (12)$$

The load voltage of the three-phase SEIG is,

$$V_L = \frac{V_t\sqrt{\left(\sigma^2 - 2\sigma\cos(\beta+\alpha)\sin\sigma + \sin^2\sigma\right)}}{\pi} \quad (13)$$

where α, $\sigma(\sigma=\beta-\alpha)$ and β are the triggering angle, the conduction angle and the extinction angle of the AC-LVR thyristor, respectively.

7. Simulation and Experimental Results of the Proposed Voltage Regulation Scheme

The generated terminal voltage of the three-phase SEIG falls steeply when the load power increases or the prime mover speed decreases[1-7]. The static VAR compensator composed of TSC and FC is used to increase the allowable range of the required power from the three-phase SEIG. The AC-LVR is applied to regulate the DC load voltage so that it falls within the reference load voltage. Fig. 11 shows the simulation of the DC load voltage and the AC-LVR triggering angle responses using the AC-LVR for the three-phase SEIG with DC load variations. Fig. 12 depicts the experimental responses of the DC load voltage and the AC-LVR triggering angle. The PI compensator controls the AC-LVR triggering angle until the load voltage, which is affected by load and prime mover speed variations, is regulated to the reference voltage. At full load, an additional excitation capacitance from the TSC type is switched on. Figs. 13 and 14 show the simulation and experimental responses of the DC load voltage and the AC-LVR triggering angle responses, respectively, when the three-phase SEIG is excited by the SVC composed of FC in parallel with TSC.

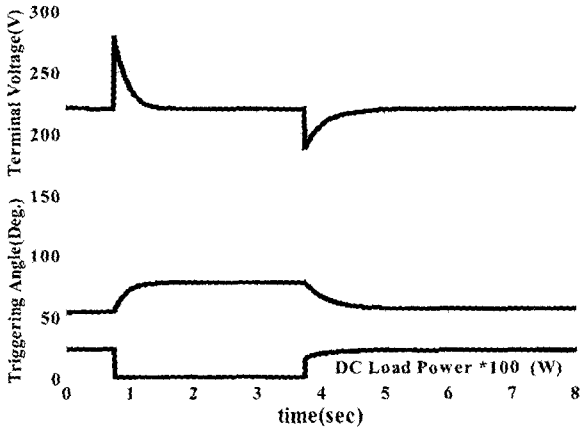

Fig.11 DC Load voltage and AC-LVR thyristor triggering angle responses with DC load variations

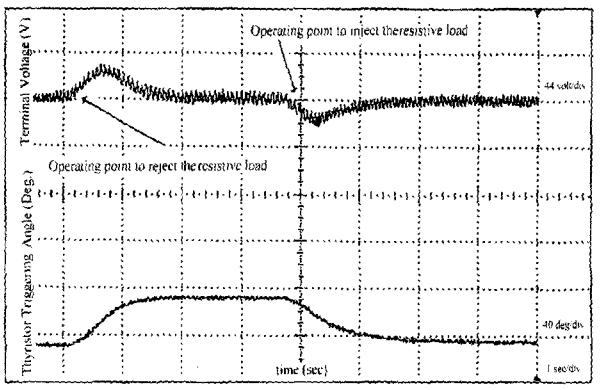

Fig.12 Experimental DC load voltage and AC-LVR thyristor triggering angle responses with DC load variations

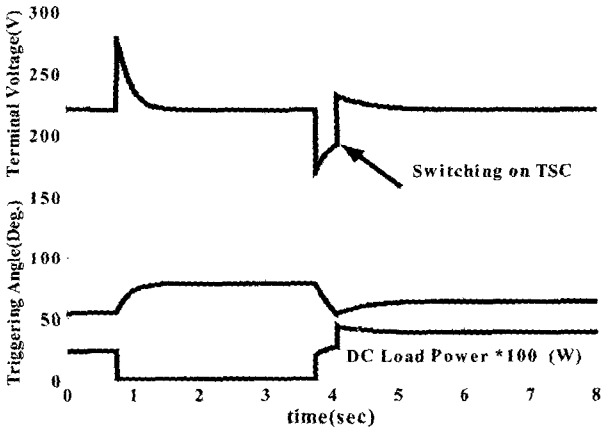

Fig.13 DC Load voltage and AC-LVR thyristor triggering angle responses with DC load variations(no-load/full load)

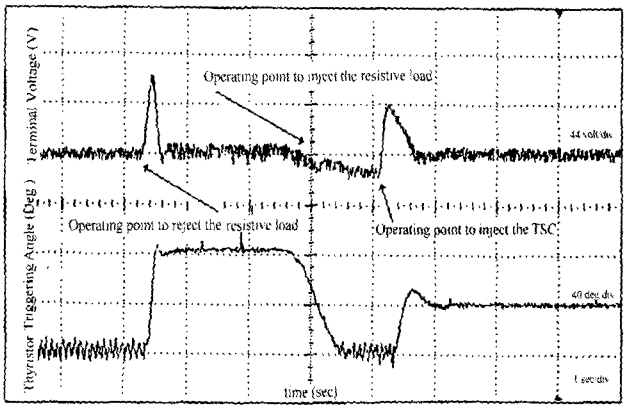

Fig.14 Experimental DC load voltage and AC-LVR thyristor triggering angle responses with DC load variations (no-load/full load)

By increasing the speed of the prime mover from 1300 r/min to 1500 r/min and then decreasing it to 1000 r/min, Fig.15 depicts the experimental responses of the load voltage and the AC-LVR thyristor triggering angle. The three-phase SEIG is supplying a DC load with the AC-LVR controlled by a PI compensator. From the experimental results of the three-phase SEIG load voltage and the AC-LVR thyristor triggering angle responses, we have demonstrated that the circuit can handle a wide range of prime mover speeds such as one might expect from a wind turbine.

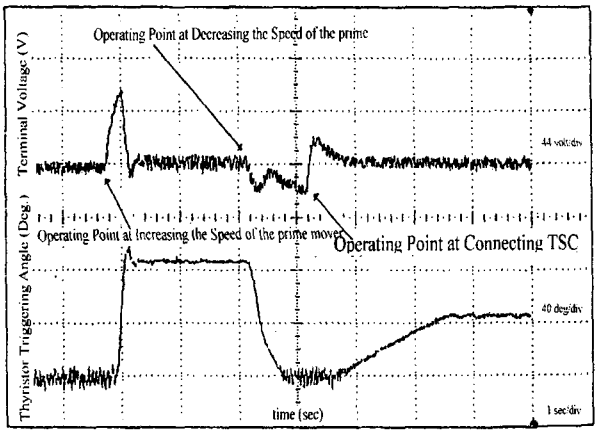

Fig. 15 Experimental load voltage response of SEIG excited by TSC and FC and AC-LVR thyristor triggering angle response with prime mover speed variations

8. Conclusions

In this paper, we have demonstrated the dynamic performance responses and experimental results of a three-phase SEIG directly connected to a full-bridge diode rectifier circuit for dc utilization. We have also derived its d-q model in a stationary reference frame. Moreover, this paper also dealt with the SVC and the AC-LVR for the voltage regulation of the three-phase SEIG. Changes to the DC load and the speed of the prime mover were applied to build and test the proposed SVC-based feedback control implementation system. A three-phase SEIG prototype set-up excited by SVC and AC-LVR was established. We demonstrated experimentally that a three-phase SEIG provides a simple method for regulating voltage for renewable energy applications. This proposal for using a SVC and an AC-LVR to excite and control the induction generator voltage of an analogous PI closed loop feedback control system is cheap, reliable, highly efficient and does not require position-sensing systems.

Appendix

$$\dot{Z}_{rm} = \frac{(jX_m)\dot{Z}_r}{\dot{Z}_r + jX_m} \tag{A1}$$

$$\dot{Z}_{mq} = \frac{R_s}{f} + jX_{ls} \tag{A2}$$

$$\dot{Z}_{qr} = \frac{-j\frac{X_C + X_{TSC}}{f^2}(R_{Lrf} + jX_{Lrf})}{R_{Lrf} + j(X_{Lrf} - \frac{X_C + X_{TSC}}{f^2})} \tag{A3}$$

$$R_{Lrf} = \pi \frac{\frac{R_L}{f}\cos(\tan^{-1}\theta) + X_L \sin(\tan^{-1}\theta)}{\sqrt{\sigma^2 - 2\sigma\cos(\beta+\alpha)\sin\sigma + \sin^2\sigma}}$$

$$X_{Lrf} = \pi \frac{-\frac{R_L}{f}\sin(\tan^{-1}\theta) + X_L \cos(\tan^{-1}\theta)}{\sqrt{\sigma^2 - 2\sigma\cos(\beta+\alpha)\sin\sigma + \sin^2\sigma}}$$

$$\theta = \tan^{-1}\left[\frac{\sin(\beta+\alpha)\sin(\sigma)}{\sigma - \cos(\beta+\alpha)\sin\sigma}\right],$$

$$\dot{Z}_r = \frac{R_r}{f - \upsilon} + jX_{lr}$$

$A_0 = T_0 G_2$,
$A_1 = G_3 T_0 + G_2 T_1 + G_0 R_R + X_{lr} X_C G_2$,
$A_2 = G_3 T_1 + G_2 T_2 + G_0 X_R + G_1 R_R + X_{lr}(X_C G_3 - R_S G_2)$,
$A_3 = G_3 T_2 + G_2 T_3 + G_1 X_R - X_{lr}(R_1 G_3 + X_1 G_2)$,
$A_4 = G_3 T_3 - X_{lr} X_1 G_3$,

$D_0 = T_0 G_0$,
$D_1 = G_0 T_1 + G_1 T_0 - F_0 X_{lr} G_2$,
$D_2 = G_0 T_2 + G_1 T_1 - F_1 X_{lr} G_2 - F_0 X_{lr} G_3$,
$D_3 = G_0 T_3 + G_1 T_2 - F_2 X_{lr} G_2 - F_1 X_{lr} G_3$,
$D_4 = G_1 T_3 - F_3 X_{lr} G_2 - F_2 X_{lr} G_3$,
$D_5 = -F_3 X_{lr} G_3$,
$C_0 = G_0 F_0$,
$C_1 = G_0 F_1 + G_1 F_0 + T_0 X_{lr} G_2$,

$C_2=G_0F_2+G_1F_1+X_{lr}(G_2T_1+G_3T_0)$,
$C_3=G_0F_3+G_1F_2+X_{lr}(G_2T_2+G_3T_1)$,
$C_4=G_1F_3+X_{lr}(G_2T_3+G_3T_2)$,
$C_5=X_{lr}G_3T_3$, $B_0=G_2F_0-X_cG_0$,

$B_1=G_3F_0+G_2F_1-X_cG_1+R_1G_0$,
$B_2=G_3F_1+G_2F_2+X_{lr}G_2R_1+X_1G_0+R_1G_1$,
$B_3=G_3F_2+G_2F_3+X_{lr}(G_3R_R+G_2X_R)+X_1G_1$,
$B_4=G_3F_3+X_{lr}G_3R_R$,

$T_0=R_1X_C$,
$T_1=X_C(X_1+X_{ls})+R_RX_{ls}$,
$T_2=X_RR_S-X_{ls}R_1$,
$T_3=-X_{ls}X_1$,

$F_0=-X_C(R_R+R_1)$,
$F_1=-X_CX_R+R_SR_1$,
$F_2=X_{ls}R_R+X_1R_S$,
$F_3=X_{ls}X_R$,

$R_R=R_Lcos[tan^{-1}(a_1/b_1)]/C_n$,
$R_1=-R_Lsin[tan^{-1}(a_1/b_1)]/C_n$,
$X_R=X_Lcos[tan^{-1}(a_1/b_1)]/C_n$,
$X_1=-X_Lsin[tan^{-1}(a_1/b_1)]/C_n$,

$\varphi=tan^{-1}(X_L/R_L)$,

$$C_n=\left(\sqrt{\sigma^2-2\sigma cos(\beta+\alpha)sin\sigma+sin^2\sigma}\right)/\pi$$

$G_0=3E_1^2/\omega_s$, $G_1=\upsilon_0R_r$, $G_2=-\tau_0$, $G_3=\upsilon_0$, $\sigma=\beta-\alpha$, $\beta=\pi+\varphi$

$Y_0=A_0D_0+B_0C_0$,
$Y_1=A_0D_1+A_1D_0+B_0C_1+B_1C_0$,
$Y_2=A_0D_2+A_1D_1+A_2D_0+B_0C_2+B_1C_1+B_2C_0$,
$Y_3=A_0D_3+A_1D_2+A_2D_1+A_3D_0+B_0C_3+B_1C_2+B_2C_1+B_3C_0$,
$Y_4=A_0D_4+A_1D_3+A_2D_2+A_3D_1+A_3D_1+A_4D_0+B_0C_4+B_1C_3$
$+B_2C_2+B_3C_1+B_4C_0$,
$Y_5=A_0D_5+A_1D_4+A_2D_3+A_3D_2+A_4D_1+B_0C_5+B_1C_4+B_2C_3$
$+B_3C_2+B_4C_1$,
$Y_6=A_1D_5+A_2D_4+A_3D_3+A_4D_2+B_1C_5+B_2C_4+B_3C_3+B_4C_2$,
$Y_7=A_2D_5+A_3D_4+A_4D_3+B_2C_5+B_3C_4+B_4C_3$,
$Y_8=A_3D_5+A_4D_4+B_3C_5+B_4C_4$,
$Y_9=A_4D_4+B_4C_4$,

References

[1] A.K.Aljabri and A.I.Alolah, "Capacitance Requirement for Isolated Self-Excited Induction Generator", IEE Proceedings, Part B, Vol.137, No.3, pp.154-159, May, 1990.

[2] T. Ahmed, O. Noro, E. Hiraki and M. Nakaoka," Terminal Voltage Regulation Characteristics by Static VAR Compensator for a Three-Phase Self-Excited Induction Generator", IEEE Trans. on Industry Applications, Vol.40, No.4, July / August 2004.

[3] Michael B. Brennen and Alberto Abbondanti," Static Exciters for Induction Generator" IEEE Trans. on Industry Applications, Vol.IA-13, No.5, September/ October, 1977.

[4] Marcos S. Miranda, Renato O. C. Lyra and Selenio R. Silva, "An Alternative Isolated Wind Electric Pumping System Using Induction Machines", IEEE Trans. on Energy Conversion, Vol.14, No.4 pp.1611-1616, December, 1999.

[5] Ermis, H.B.Erton, M.Demirekler, B.M.Saribatir, Y.Uctvg, M.E.Sezer and I.Cadirici," Various Induction Generator Schemes for Wind-Electricity Generation", Electric Power Systems Research, Vol.23, pp.71-83, 1992

[6] A.A.Shaltout and M.A.Adel-Halim, "Solid State Control of Wind-Driven Self-Excited Induction Generator", Electric Machines and Power Systems, Vol.23, pp.571-582,1995

[7] E. Suarez and G. Bortolotto, "Voltage-Frequency Control of A Self-Excited Induction generator", IEEE Trans. on Energy Conversion, Vol.14, No.3 pp.394-401, September, 1999.

[8] R. Leidhold, G. Garcia and M.I. Valla, "Induction generator Controller Based on the Instantaneous Reactive Power Theory", IEEE Trans. on Energy Conversion, Vol.17, No.3 pp.368-373, September, 2002.

[9] M. Naidu and J. Walters, "A 4-kW 42-V Induction-Machine-Based Automotive Power Generation System With a Diode Bridge Rectifier and a PWM Inverter", IEEE Trans. on Industry Applications, Vol.39, No.5 pp.1287-1293, September/October, 2003.

[10] IEEE Special Stability Controls Working Group Report, "Static VAR Compensator Models for Power Flow and Dynamic Performance Simulation ", IEEE Transactions on Power Systems, Vol.9, No.1, February, 1994.

Tarek Ahmed received his M.Sc. degree in electrical engineering from the Electrical Engineering Department, Faculty of Engineering, Assiut University, Egypt in 1998. He is an assistant lecturer in the Electrical Engineering Department, Faculty of Engineering, Assiut University, Assiut, Egypt. He is currently a Ph. D. candidate with the Power Electronic System and Control Engineering Laboratory in the Division of Electrical and Electronic Systems Engineering at the Graduate School of Science and Engineering, Yamaguchi University, Yamaguchi, Japan. He received Paper Awards from the Institute of Electrical Engineers of Japan (IEE-J) in 2003 and

in 2004. His research interests are in the new applications of advanced high frequency resonant circuits and systems with renewable energy related soft switching PWM rectifiers and sine wave PWM inverter power conditioners. Mr. Ahmed is a student-member of the Institute of Electrical and Electronics Engineers of the USA (IEEE-USA), the Institute of Electrical Engineering and Installation of Engineers (IEIE-Japan), the Institute of Electrical Engineers (IEE-Japan) and the Japan Institute of Power Electronics (JIPE).

Katsumi Nishida received his B.S., and M.S. degrees in electrical engineering from the Tokyo Institute of Technology, Tokyo in 1976 and 1978, respectively. He received his Ph.D. degree from the Division of Electrical and Electronic Systems Engineering at the Graduate School of Science and Engineering, Yamaguchi University, Yamaguchi, Japan in 2002. He is engaged in research on power factor correction of PWM converters and current control of the three-phase active power filters using the dead-beat technique and the adaptive signal processing technique. Dr. Nishida is a member of the Institute of Electrical and Electronics Engineers of the USA (IEEE-USA), the Institute of Electrical Engineers of Japan (IEE-Japan) and the Japan Institute of Power Electronics (JIPE).

Mutsuo Nakaoka received his Dr.-Eng. degree in Electrical Engineering from Osaka University, Osaka, Japan in 1981. He joined the Electrical and Electronics Engineering Department of Kobe University, Kobe, Japan in 1981 and served as a professor of the Department of Electrical and Electronics Engineering at the Graduate School of Engineering, Kobe University, Kobe, Japan until 1995. He is currently working as a professor in the Electrical and Electronics Engineering Department at the Graduate School of Science and Engineering, Yamaguchi University, Yamaguchi, Japan. His research interests include application developments of power electronics circuits and systems. He has received more than ten awards such as the 2001 premium prize paper award from IEE-UK, the 2001 and 2003 Best Paper Awards from IEEE-IECON, the 2000 third paper award from IEEE-PEDS, the 2003 James Melcher Prize Paper award from IEEE-IAS. He is now a chairman of the IEEE Industrial Electronics Society Japan Chapter. Dr. Nakaoka is a member of the Institute of Electrical Engineering Engineers of Japan, the Institute of Electronics, Information and Communication Engineers of Japan, the Institute of Illumination Engineering of Japan, the European Power Electronics Association, the Japan Institute of Power Electronics, the Japan Society of Solar Energy, the Korean Institute of Power Electronics, IEE-Korea and IEEE.